Available online at www.sciencedirect.com

SciVerse ScienceDirect

Ceramics International 38 (2012) 4081–4096

CERAMICS INTERNATIONAL

www.elsevier.com/locate/ceramint

Influence of the intermixed interfacial layers on the thermal cycling behaviour of atmospheric plasma sprayed lanthanum zirconate based coatings

Ramachandran C.S. [a,*], Balasubramanian V. [a], Ananthapadmanabhan P.V. [b], Viswabaskaran V. [c]

[a] *Department of Manufacturing Engineering, Annamalai University, Annamalai Nagar 608 002, Tamil Nadu, India*

[b] *Plasma Spray Technologies Section (PSTS), Laser and Plasma Technology Division (L&PTD), Bhabha Atomic Research Centre (BARC), Anu Shakthi Nagar, Trombay, Mumbai 400 085, Maharashtra, India*

[c] *# 27A, 14th Link Road, 3rd Cross, Venkateswara Colony, Nehru Nagar, Kottivakkam, Chennai 600 041, Tamil Nadu, India*

Received 25 December 2011; received in revised form 22 January 2012; accepted 25 January 2012
Available online 1 February 2012

Abstract

In application as a thermal barrier coating (TBC), yttria stabilised zirconia (YSZ) approaches some limits of performance. To further enhance the efficiency of gas turbines, higher temperature capability and a longer lifetime of the coating are needed for the next generation of TBCs. Pyrochlore oxides of general composition, $A_2B_2O_7$, where A is a 3^+ cation (La to Lu) and B is a 4^+ cation (Zr, Hf, Ti, etc.) have high melting point, fair coefficient of thermal expansion, and low thermal conductivity which make them suitable for applications as high temperature thermal barrier coatings. Among those oxide materials lanthanum zirconate (LZ/$La_2Zr_2O_7$) offers very attractive properties. This work describes the fabrication, microstructure and high temperature (1280 °C) thermal cycling behaviour of lanthanum zirconate coatings with five different coating architectures, deposited using atmospheric plasma spray process. The coating architecture which had five layers with two intermixed interlayers had much longer life time than other considered architectures. The coatings were characterised using X-ray diffraction, energy dispersive spectrometry, optical and scanning electron microscopy, before and after thermal cycling tests, to study the coating failure mechanisms.

Keywords: B. Interfaces; C. Thermal shock resistance; D. ZrO_2; E. Engine components

1. Introduction

Thermal barrier coatings (TBCs) have been widely used in advanced aircraft and industrial gas-turbine engines in order to enhance the reliability and durability of hot-section metal components as well as the efficiency of engines [1]. The selection of TBC materials is restricted by some basic requirements such as: (1) high melting point, (2) no phase transformation between room temperature and operation temperature, (3) low thermal conductivity, (4) chemical inertness, (5) thermal expansion match with the metallic substrate, (6) good adherence to the metallic substrate, and (7) low sintering rate of the porous microstructure [2]. Therefore, the number of materials that can be used as TBCs is very limited. The state of the art TBC material is 8YSZ, which can hardly be used for long term application above 1200 °C due to the sintering and phase transformation [3]. There are several ceramic materials that have been evaluated as high temperature TBC materials, and lanthanum zirconate is one of the most promising among them. The properties of high-melting point, phase stability up to its melting point, low thermal conductivity, low sintering ability and oxygen-non-transparent are the major reasons for the belief that lanthanum zirconate has potential as TBC material for high-temperature applications [4].

Vassen et al., studied the thermo-physical properties of LZ material and successfully produced a coating through APS technique [5]. Observation from their results clearly underlines that LZ has good potential as a new material for advanced TBCs, even though it has lower Young's modulus and thermal expansion than that of YSZ. Furthermore, their results proved that the thermal conductivity of LZ which is approximately

* Corresponding author. Tel.: +91 4144 230382; fax: +91 4144 239734/238275; mobile: +91 09843892693.
E-mail address: csrcn@rediffmail.com (R. C.S.).

0272-8842/$36.00
doi:10.1016/j.ceramint.2012.01.066

20% lower than that of YSZ is favourable at elevated temperatures, and it also shows excellent thermal stability. Subsequently, Hui Dai et al., investigated double-ceramic-layer (DCL) APS coatings with various thickness ratios composed of YSZ (6–8 wt.% $Y_2O_3 + ZrO_2$) and lanthanum zirconate (LZ, $La_2Zr_2O_7$) [6]. Their results indicated that the thermal cycling lives of the DCL coatings depend strongly on the thickness of YSZ. When its thickness is between 150 and 200 μm, the DCL coating (980 cycles) has a longer thermal cycling life than the single layer YSZ coating (825 cycles). Xu et al., compared the thermal cycling lives of LZ, YSZ and DLC coatings deposited by EBPVD process [7]. The DCL coating withstood 2913 cycles which corresponded to a total cycling time of 1699 h exhibiting a significant improvement in the thermal cycling life. Meanwhile, its thermal cycling life is not only much longer than that of LZ, but also approximately 30% longer than that of 8YSZ. The long lifetime of the DCL coating can be mainly attributed to the effective reduction of the thermal expansion mismatch between BC and LZ coating, and from the favourable thermal gradient condition caused by the low thermal conductivity of LZ. Common double ceramic-layered TBCs, such as LZ/YSZ [7], and LZ/$La_2Ce_{3.25}O_{9.5}$ [8] have been proven to exhibit reduced oxygen permeation and are able to prolong the thermal cycling life slightly better than the traditional duplex coatings.

Unfortunately, weak bond strengths and high residual stresses between the two ceramic layers resulting from strain mismatch still remain as serious problems. These result in premature, spontaneous failures with large-area spallations under thermal and mechanical loads for double ceramic layered TBC systems. Hence, this investigation was carried out to clarify the effects of different coating architectures with intermixed interfacial layers on the thermal cycling life of LZ based coatings, and to study the failure mechanism. Further, the number of cycles withstood by a TBC under thermal cycling conditions are decided by the factors namely the bond coat composition, the bond coat deposition technique, the bond coat thickness, the ceramic coating deposition technique, the volume percentage of porosity, morphology of the coating, thickness of the ceramic coating, the thermal cycling technique, the peak temperature, the bottom temperature, dwell time at the peak and the bottom temperature, the heating and the cooling rates, the cycling pattern, the criterion for the termination of test, etc. Since the aforesaid factors are different in the literature survey and in the current investigation, the results thus derived cannot be compared as such and they are investigation and system specific. The thermal cycling tests mentioned above were used by the authors only to categorise the coatings according to their spallation resistance. To put these kinds of TBCs under service, one has to carry out engine tests by coating these TBC materials on to the actual turbine components (blades, combustor cans, engine housing, etc.) and run the engine until visible cracking/spallation of the coating occurs. Furthermore, the five layered architecture with intermixed interfacial layers considered in the present investigation is truly unique in nature and has not been trialled/reported by others.

2. Experimental

2.1. Coating deposition

An agglomerated and sintered yttria stabilised zirconia (YSZ) spherical powder with size ranging between 10 and 45 μm [Make: H.C. Stark, AMPERIT 827.054 powder (ZrO_2, 7 wt.% Y_2O_3)] was used. Since the lanthanum zirconate (LZ) powder is not commercially available, the same was prepared in our laboratory. The method of preparing the plasma spray quality lanthanum zirconate power is available in our previously published paper [9]. The substrate coupons were of nickel based super alloy Inconel 738 material (BM). The dimensions of the substrate (BM) coupons were 25.4 mm × 12.2 mm × 3 mm. The corners and the edges of the substrate (BM) coupons were chamfered and rounded prior to grit blasting. Grit blasting was carried out using corundum grits of 16 mesh size using an automated high pressure suction blasting system (Make: MEC; India. Model: MEC SUBC MK III) to achieve a roughness average (R_a) of 9–11 μm. The surface roughness was measured using a diamond stylus surface roughness tester (Make: Mitutoyo, Japan. Model: SFTT301). The ceramic powders were plasma sprayed over NiCrAlY (Ni–22Cr–10Al–1Y, Make: Praxair NI-343, Size: 10–45 μm) bond coat (BC), which was previously deposited using HVOF (Make: MEC, India. Model: MEC HIPOJET 7100) process on to the grit blasted Inconel 738 coupons (BM). The coatings were made on all the six sides of the grit blasted (BM) coupons. The plasma spray deposition of the YSZ and the synthesised LZ powders were carried out using a semi-automatic 40 kW IGBT-based Plasmatron (Make: Ion Arc Technologies, India. Model: APSS-II). The investigation was started to compare the thermal cycling lives of the duplex YSZ and LZ coatings. But, the intrinsic low coefficient of expansion and the low fracture toughness of the LZ coating, compared to YSZ coatings as inferred in the literature [10], made the authors try different coating architectures to find whether the thermal cycling life of the LZ coatings could be improved. The various coating architectures considered for the investigation, are shown in Fig. 1. The total thickness of all the coatings, were kept constant at 500 μm. Since the intermixed layers are involved, the two powder mixtures namely the LZ + YSZ and the YSZ + NiCrAlY powder mixtures (50 + 50 wt.%) were mixed respectively in a ball mill for 4 h in dry condition with zirconia balls as the mixing medium. The porosity levels of the ceramic coatings were maintained between 13 and 15 vol% by appropriately modifying the APS process parameters. The process parameter settings to deposit the coatings using APS and HVOF spray processes are shown in Table 1. The deposited coatings as such are shown in Fig. 2.

2.2. Evaluation of mechanical properties of the coatings

Customary metallographic procedures were adopted to polish the cross-section of the coatings. The cross-sectional images of the coatings were captured using optical microscope (Make: Meiji, Japan. Model: MIL-7100). The porosity was

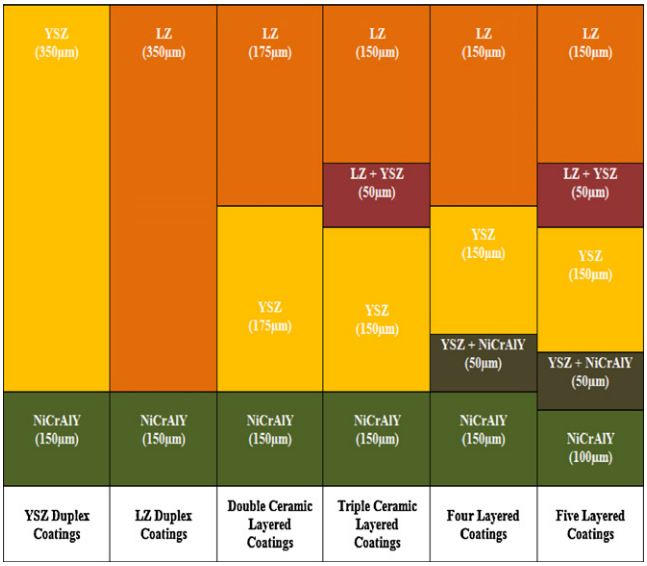

Fig. 1. Considered coating architectures.

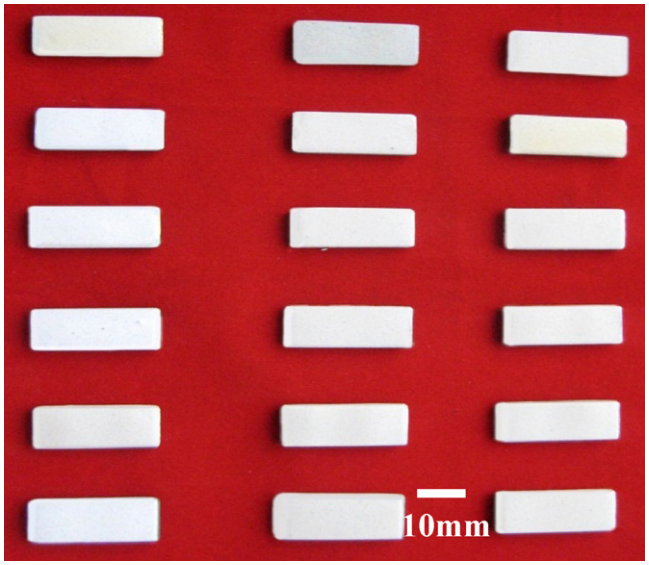

Fig. 2. Coatings prepared for thermal cycling test.

analysed as per ASTM B 276 standard on the polished cross section of the coating using the same optical microscope equipped with image analysing system. The coatings were also subjected to SEM and EDAX analysis (Make: Quanta, Switzerland. Model: 3D FEG-I). The phases present in the coatings were determined by XRD analysis (Make: Rigaku, Japan. Model: ULTIMA-III). The microhardness measurements were made on the polished cross-sections of the coatings, using a Vickers microhardness tester (Make: Shimadzu, Japan. Model: HMV-2T). A load of 300 g and a dwell time of 15 s were used to evaluate the hardness. Hardness values were measured at 10 random locations on the polished cross-section of a coating. The tensile bond strength test was carried out as per ASTM C 633 standard using a universal testing machine (Make: FIE Blue Star, India. Model: UNITEK-94100). A commercially available heat curable epoxy was used as an adhesive, to test the coated specimens. The method of conducting the bond strength test and the analysis thereof can be referred in our previously published paper [11].

2.3. Thermal cycling test method for the coatings

The thermal cycling test was carried out, using a 1800 °C tubular sintering furnace (Make: VBCC, India. Model: VBHTSF-1800MF12). The coupons for thermal cycling were placed on a zircar plate and inserted directly into the hot zone (Ø70 mm × 150 mm) having a temperature of 1280 °C, in which the coupons were exposed to the aforesaid temperature for 50 min, followed by cooling the coupons for 10 min under a diffused air cooling arrangement leading to room temperature. This 1 h cycle was repeated until a 20% of the coating got peeled off and the corresponding number of cycle was recorded as the life time of the coating. Further, during thermal cycling test, the weight difference of the coatings were measured once in every 15 cycles, by means of a precision weighing machine (Make: Shimadzu, Japan. Model: AW 320) with 0.01 mg of resolution to determine the specific weight gain of the coatings.

3. Results

The cross-sectional micrographs of the coatings before thermal cycling test are presented in the Figs. 3–14. The duplex YSZ and LZ coatings (Figs. 3–6) display a sharp and clear interface between the ceramic coat and the BC. The double ceramic layered coating also exhibits the same kind of clear interface between the LZ–YSZ interface and YSZ–BC interface as seen in Figs. 7 and 8. The LZ–YSZ interface of the triple ceramic layered coating (Figs. 9 and 10) and the YSZ–BC interface of the four layered coatings (Fig. 11) have no sharp interface, due to the induction of a layer with intermixed materials of the top and bottom layers. In the same way, the LZ–YSZ coating interface and the YSZ–BC interface of the five layered coating do not exhibit a clear interface (Figs. 12–14) due to the presence of the 50 μm thick intermixed interfacial

Table 1
Process factors and their respective levels.

APS/HVOF factors	YSZ (APS)	LZ (APS)	NiCrAlY (HVOF)
Power (kW)	26	24	–
Stand-off distance (mm)	115	115	210
Primary/Secondary gas flow rate (APS: Ar/N_2, HVOF: Air/Butane/O_2) (lpm)	38/5	38/4	950/80/250
Powder feed rate (gpm)	21	21	38
Carrier gas flow rate (APS: Ar, HVOF: O_2) (lpm)	11	9	12

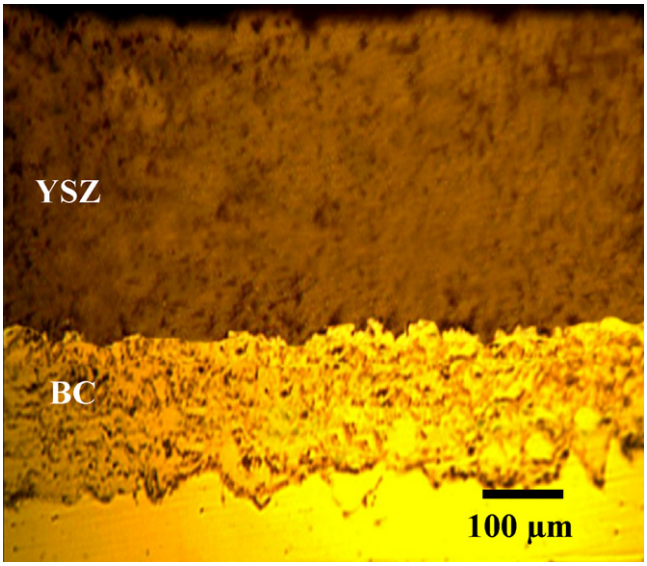

Fig. 3. Cross section of YSZ duplex coating.

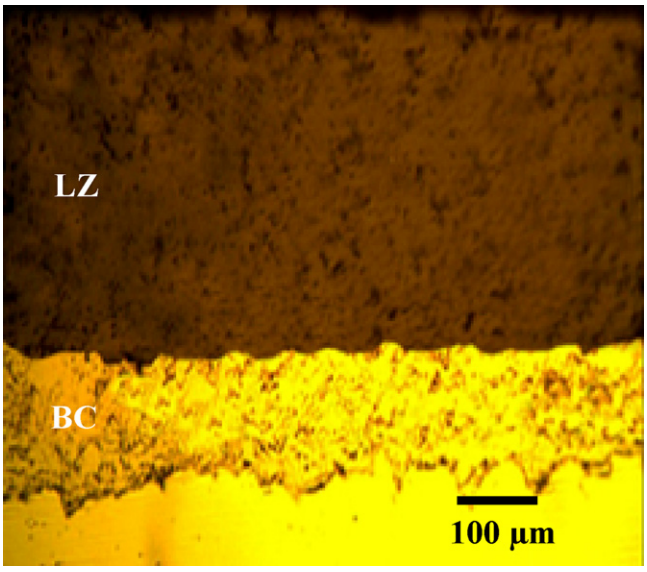

Fig. 5. Cross section of LZ duplex coating.

layers. The tensile bond strengths of the LZ, YSZ and the five layered coatings are shown in Fig. 15. The tensile bond strength of 12 MPa was recorded in the case of the LZ duplex coating; 15 MPa and 20 MPa were the bond strengths of YSZ duplex and five layered coatings, respectively.

The hardness distribution of the LZ, YSZ and five layered coatings are shown in Fig. 16. An average microhardness value of 954 $HV_{0.3}$ was recorded in the case of LZ coating and an average hardness value of 907 $HV_{0.3}$ was recorded in the case of YSZ coating. The average hardness values of the LZ–YSZ interface layer and the YSZ–BC interlayer of the five layered coating were 932 $HV_{0.3}$ and 625 $HV_{0.3}$, respectively. The thermal cyclic lifetimes of the coatings with various architectures are shown in Fig. 17. From the figure it can be said that the LZ duplex coatings exhibited the lowest thermal cycling life of 110 cycles and the five layered coating exhibited the highest thermal cycling life of 358 cycles. The specific weight gain of the YSZ coating was the highest, with a peak weight gain of 2.45 mg/cm^2 and the weight gain of the five layered coating was the lowest with a peak weight gain of 1.2 mg/cm^2 with respect to the number of thermal cycles as is shown in Fig. 18.

4. Discussions

4.1. The thermal cycling life of YSZ duplex coating

The thermal cyclic lifetime of YSZ coating was limited due to three main reasons namely, the sintering of splats, phase transformation and thick TGO layer formation. The surface

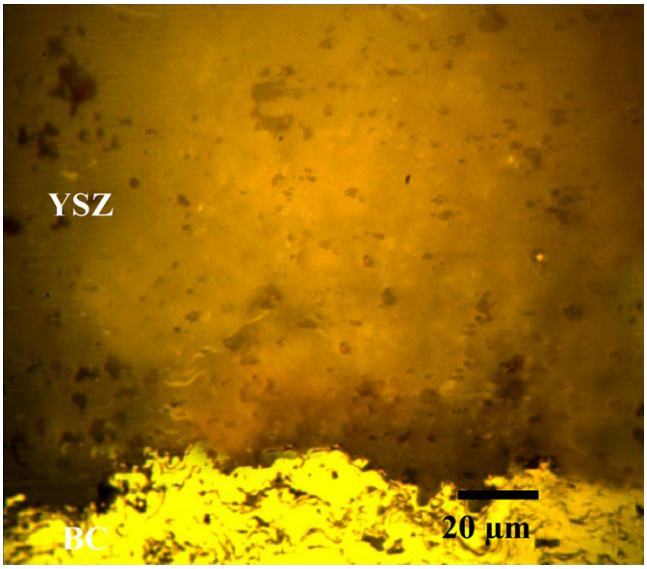

Fig. 4. Interface between YSZ coat and bond coat.

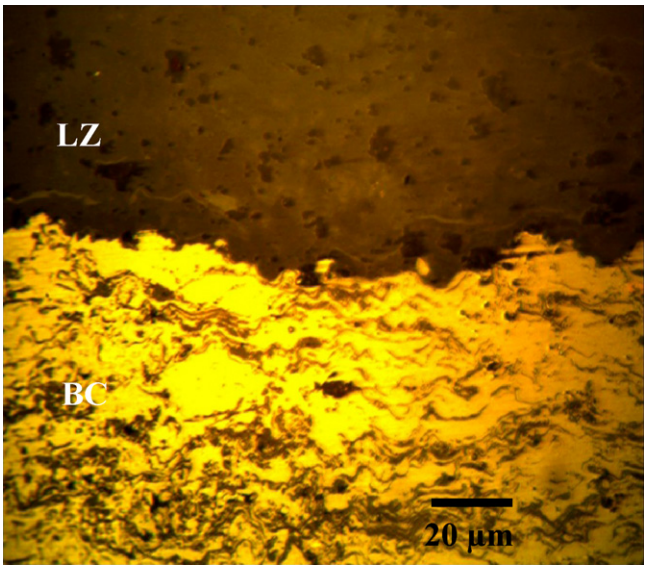

Fig. 6. Interface between LZ coat and bond coat.

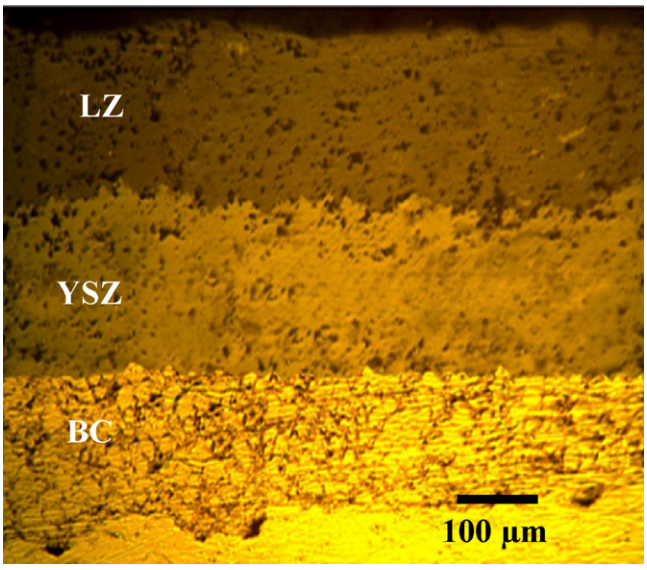

Fig. 7. Cross section of double ceramic layered coating.

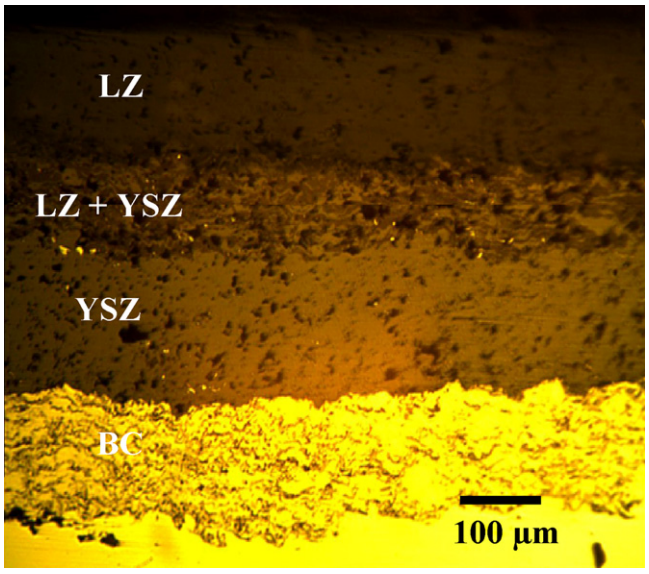

Fig. 9. Cross section of triple ceramic layered coating.

morphology of the thermal cycled and spalled YSZ duplex coating is shown in Figs. 19 and 20. Fig. 19 displays longitudinal branched cracks, which have got propagated throughout the coating surface. The high magnification image (Fig. 20) displays extensive sintering of splats and closure of open porosities.

4.1.1. Sintering of lamellae during the thermal cycling of YSZ duplex coating

As the YSZ duplex coating was exposed to 1280 °C, the sintering of the ceramic coating becomes one of the coating degradation mechanisms. Normally sintering and associated shrinkage will introduce tensile stresses, which result in transverse cracking of the ceramic perpendicular to the interface [12]. The aforementioned phenomena could be seen in Fig. 21, where a large vertical crack runs from the top of the coating up to the surface of the thermally grown oxide (TGO) layer. Sintering has been observed to effectively increase the inter splat contact area (formation of sinter necks) and to heal the intra splat micro cracks [13]. But, in this investigation the thermal cycling temperature is 1280 °C, which is 80° above the transformation temperature of the t prime phase. Hence, the prolonged cyclic exposure at such high temperature led to the change in the top coat microstructure (closure of pores) in such a way as to raise the thermal conductivity, and also to make the coating stiffer and more prone to spallation. The increased thermal conductivity and stress level might also have promoted rapid phase transformation.

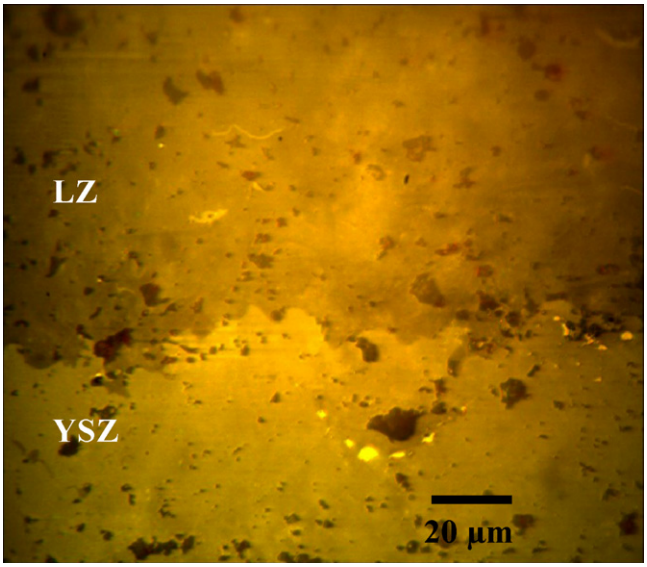

Fig. 8. Interface between LZ coat and YSZ coat of double ceramic layered coating.

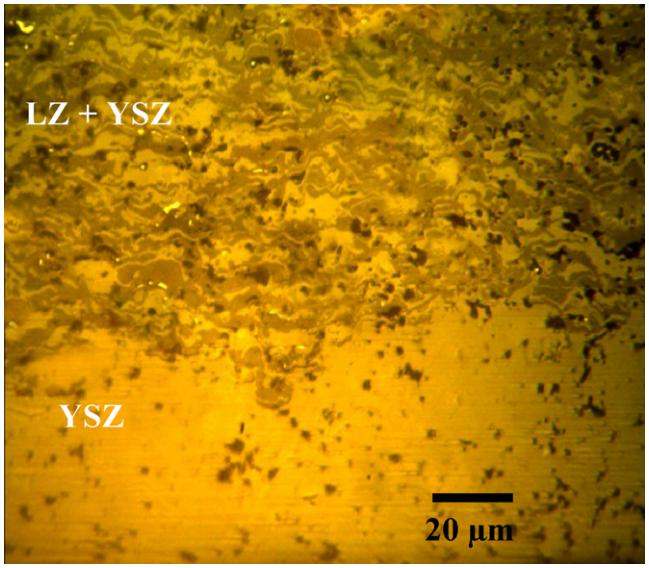

Fig. 10. Intermixed interface layer between LZ coat and YSZ coat section of triple ceramic layered coating.

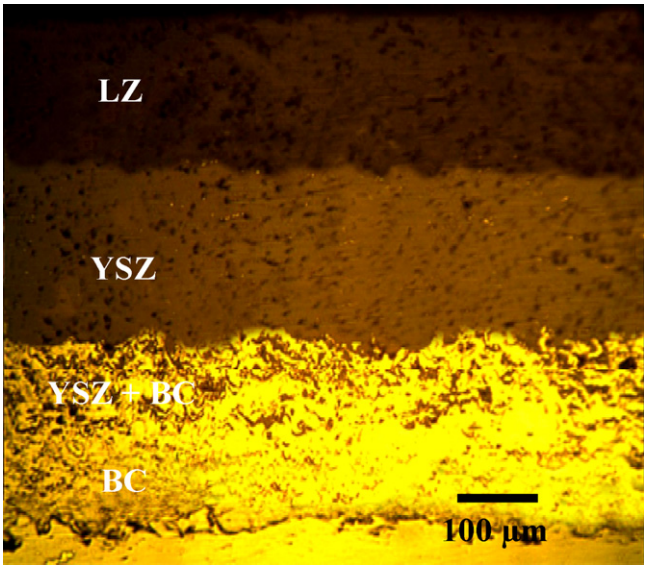

Fig. 11. Cross section of four layered coating.

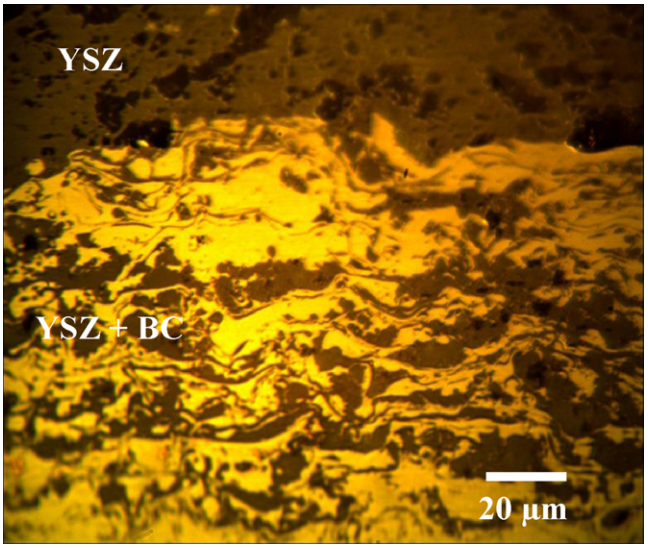

Fig. 13. Intermixed interface layer between YSZ coat and bond coat as seen below the YSZ coat.

4.1.2. Phase transformation during the thermal cycling of YSZ duplex coating

The XRD plot of the as sprayed coating shown in Fig. 22 displays the presence of t′ (tetragonal prime phase) which generally occurs due to the rapid quenching of the APS sprayed YSZ splats, whereas the XRD pattern of the thermal cycled coating (Fig. 23), shows the presence of t (tetragonal), m (monoclinic) and c (cubic) phases. The presence of m and c phases confirms that the thermally cycled YSZ duplex coating has undergone phase transformation. Prolonged exposure of YSZ coating at temperatures higher than 1200 °C leads the t′ phase present in the coating to transform into the t + m phase and c-phase. During cooling, the t-phase will further transform into the m-phase, giving rise to the formation of microcracks in the coating due to 4% volumetric expansion [14]. It has been reported that t-to-m transformation of YSZ occurs more easily under a compressive stress than under tension [15]. Because the coefficient of expansion (CTE) of t and c phase is higher than that of m phase (t: 9.6–10.7 × 10^{-6} K^{-1}; c: 7.5–13 × 10^{-6} K^{-1}; m: 6.8–8.4 × 10^{-6} K^{-1}), this variation leads to an increased residual compressive stress due to the increased mismatch of CTE between ceramic coat and BC [16]. Therefore, it could be said that the t-to-m transformation will also contribute to final spallation by increasing the compressive stress.

4.1.3. TGO formation during the thermal cycling of YSZ duplex coating

The YSZ duplex coating also exhibits thick thermally grown oxide (TGO) formation, where the separation of coating also has taken place as seen in Fig. 21. The TGO thickness is uneven throughout the YSZ–BC interface ranging between 1–8 μm

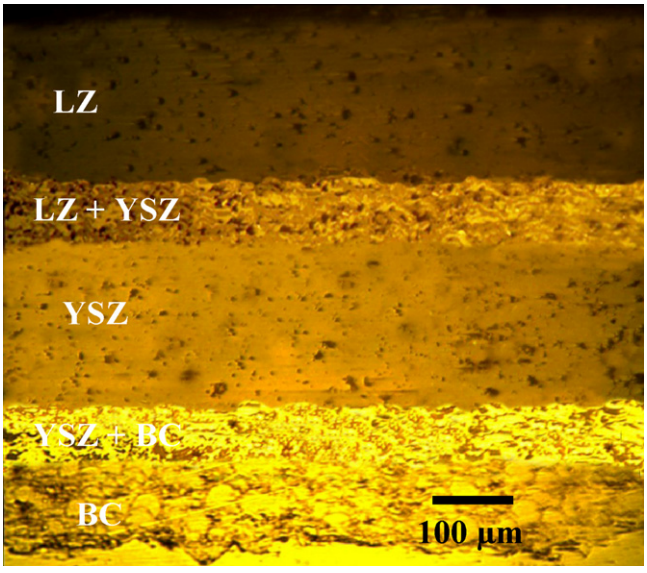

Fig. 12. Cross section of five layered coating.

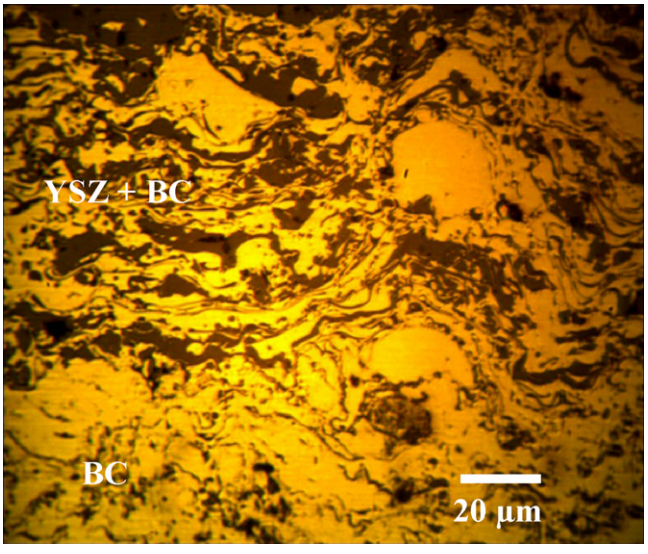

Fig. 14. Intermixed interface layer between YSZ coat and bond coat as seen above the bond coat.

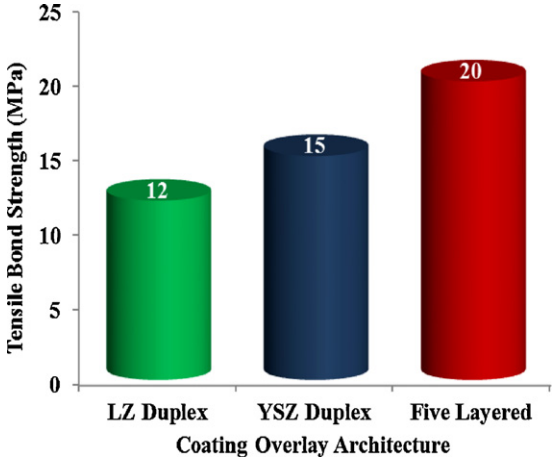

Fig. 15. Tensile bond strength of coatings.

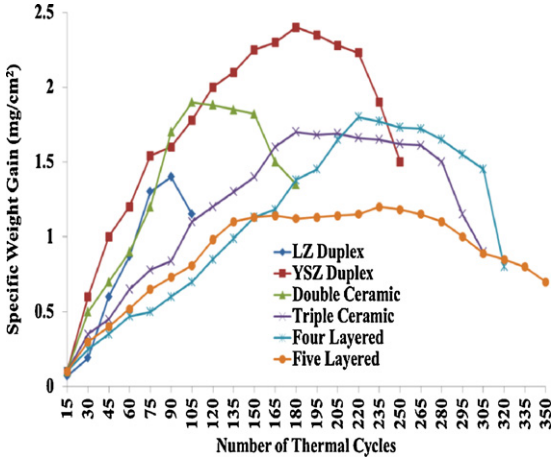

Fig. 18. Specific weight gain of coatings with respect to number of thermal cycles.

after 251 thermal cycles (Fig. 17). The specific weight gain due to oxidation of the coatings is shown in Fig. 18, which shows that the YSZ duplex coating has gained the highest specific weight. It is a known fact that the YSZ material is oxygen transparent [17]. Hence, the diffusivity of the oxygen atoms is high at higher temperatures due to oxygen transparency and formation of cracks in the coating, which in turn led to the increased thickness of the TGO layer. The EDS mapping results of the thermal cycled and spalled YSZ coating in which a small portion of YSZ was found to be adhering, is presented in Fig. 24. From the EDS mapping results, it is put forth that the alumina (Al_2O_3) is the major composition found in the TGO, but there is also formation of large clusters of other oxide mixtures. The EDS graph and mapping also confirm the aforementioned points. These oxide mixtures might be mixtures of chromia ($(Cr,Al)_2O_3$), spinels ($Ni(Cr,Al)_2O_4$), yttrium oxide ($Al_5Y_3O_{12}$ and/or $AlYO_3$) and nickel oxide (NiO) in chemical composition. The presence of such mixed oxide products has been reported by other researchers [18,19]. Once the TGO is converted from an initially continuous Al_2O_3 scale to a mixed Cr_2O_3 and $NiCr_2O_4$ oxide scale, the development of Ni/Cr rich TGO will lead to chemical inhomogeneity and degradation of the TGO/BC ending up in the spallation of

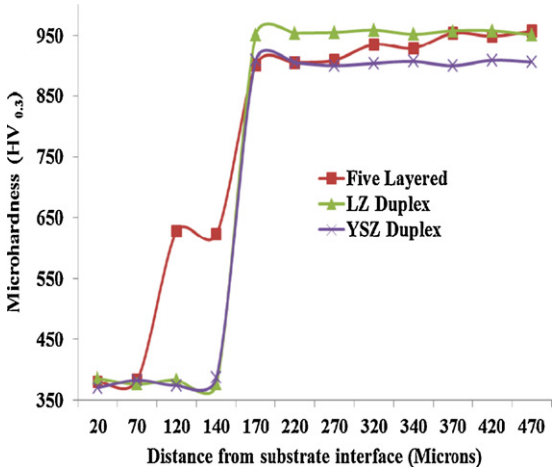

Fig. 16. Microhardness distribution in coatings.

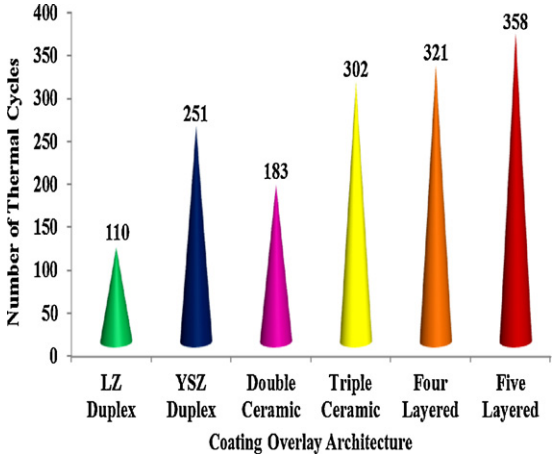

Fig. 17. Effect of coating architecture on number of thermal cycles.

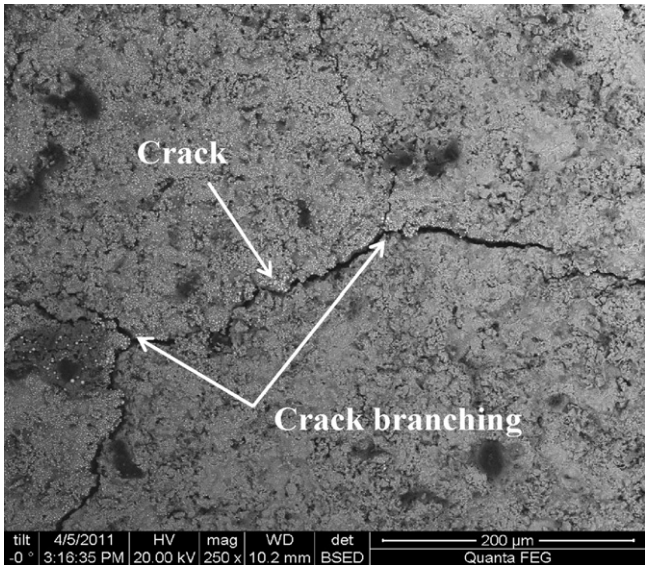

Fig. 19. Low magnification image of top surface of YSZ duplex coating after thermal cycling.

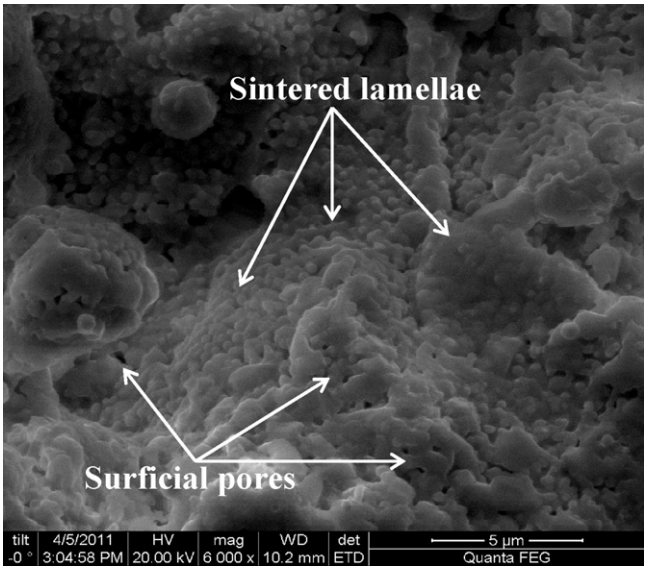

Fig. 20. High magnification image of top surface of YSZ duplex coating after thermal cycling.

coating on cooling [20,21]. In this study, the growth stresses Ni/Cr rich TGO associated with BC oxidation superimposed by thermally induced stress that occurred during thermal cycling will be one reason for the failure of YSZ duplex TBC.

4.2. The thermal cycling life of LZ duplex coating

The surface morphology of the thermal cycled and spalled LZ coating is shown in Fig. 25, which displays extensive surface cracking of LZ coatings. The closer view of the coating (Fig. 26) suggests that there are no signs of sintering, but there are multiple branched cracks emanating from the sides of a very large crack. The cross-section of the coating can be viewed in Fig. 27. In the figure one can see a large number of longitudinal and transverse cracks. This suggests that the failure of coating

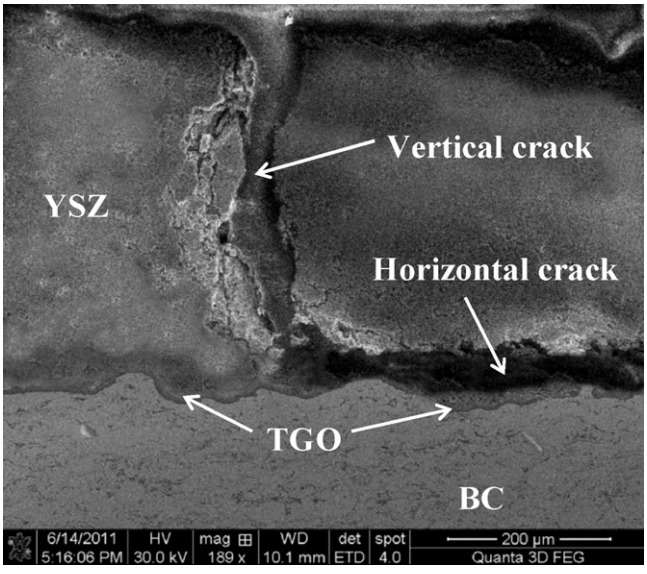

Fig. 21. Cross-sectional image of YSZ duplex coating after thermal cycling.

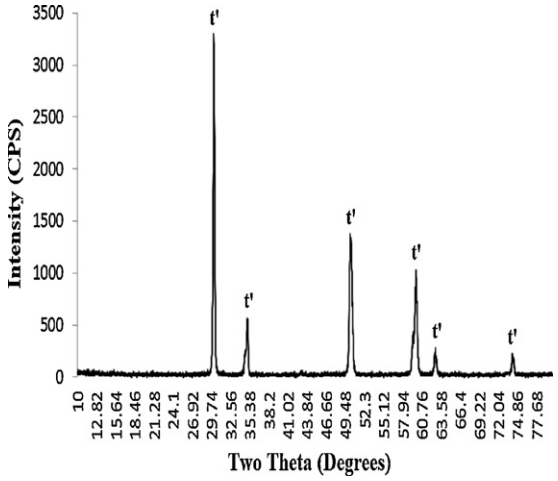

Fig. 22. XRD pattern of YSZ duplex coating before thermal cycling test.

was not due to sintering, but due to a different attribute. The XRD pattern (Fig. 28) of the LZ coating before and after thermal cycling did not show any significant variation and the cubic pyrochlore phase was maintained well without any phase transformation. The LZ coating survived the least number of cycles as illustrated in Fig. 17.

4.2.1. TGO formation during the thermal cycling of LZ duplex coating

The oxidation behaviour of the LZ coating could be seen in Fig. 18, which displays that after 40 thermal cycles the LZ coating undergoes rapid weight gain. The oxygen non-transparent nature of LZ material is a very well established phenomenon [22]. Despite the aforementioned property, the oxidative weight gain of the LZ duplex was due to the heavy cracking of the coating. The evolution of cracks led to lots of opening in the coating, leading to rapid oxidation of the BC at the ceramic coat-BC interface. It can be seen from Fig. 27 that a transverse crack is also observed above the TGO layer after thermal cycling, which implies that BC oxidation is one of the important factors for coating failure. The EDS mapping results

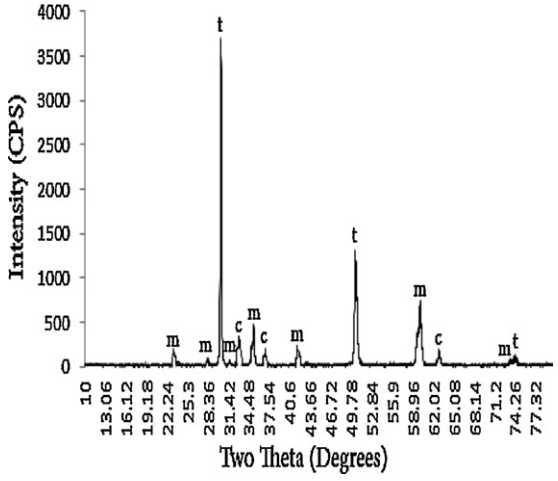

Fig. 23. XRD pattern of YSZ duplex coating after thermal cycling test.

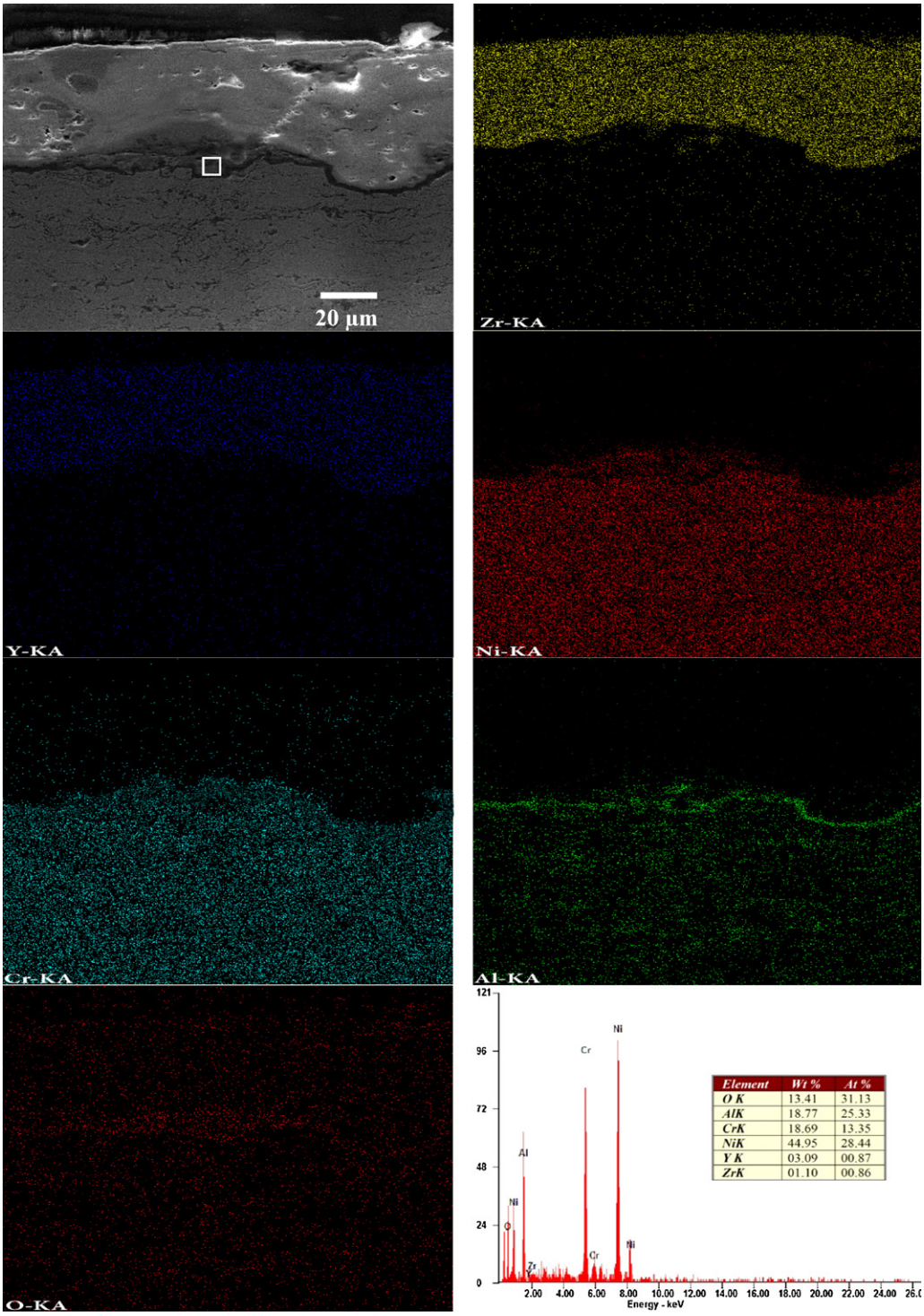

Fig. 24. EDS mapping results of YSZ duplex coating after thermal cycling test.

of thermal cycled LZ coating is shown in Fig. 29. The figure confirms the formation of a thin TGO formation and the thickness of the TGO was approximately 5–7 μm. The alumina was found to be the major ingredient and the formations of other oxides has been largely mitigated in TGO, which can be crosschecked from the elemental maps and the EDS graph. The mitigation of the formation of chromia and spinels is due to the oxygen non-transparent nature and early failure of coatings. The short thermal cycling life of the LZ coating is mainly due to the rapid propagation of numerous longitudinal and transverse cracks induced by the thermal shock created in the thermal cycling experiments. The cross-section of the coating indicates extensive cracking and the total integrity of the coating being lost. The extensive cracking is due to the low fracture toughness (LZ: 1.4 MPa $m^{1/2}$, YSZ: 1.8 MPa $m^{1/2}$) and the low coefficient of expansion (LZ: $9.1 \times 10^{-6}\ K^{-1}$, YSZ: $10.7 \times 10^{-6}\ K^{-1}$) [23]. The low fracture toughness leads to the initiation and growth of micro-cracks even with lower stress levels and the low coefficient

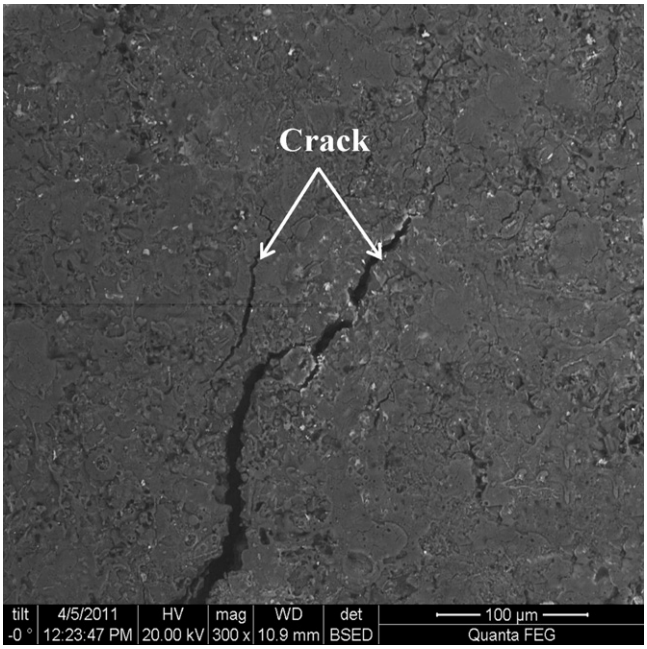

Fig. 25. Low magnification image of top surface of LZ duplex coating after thermal cycling.

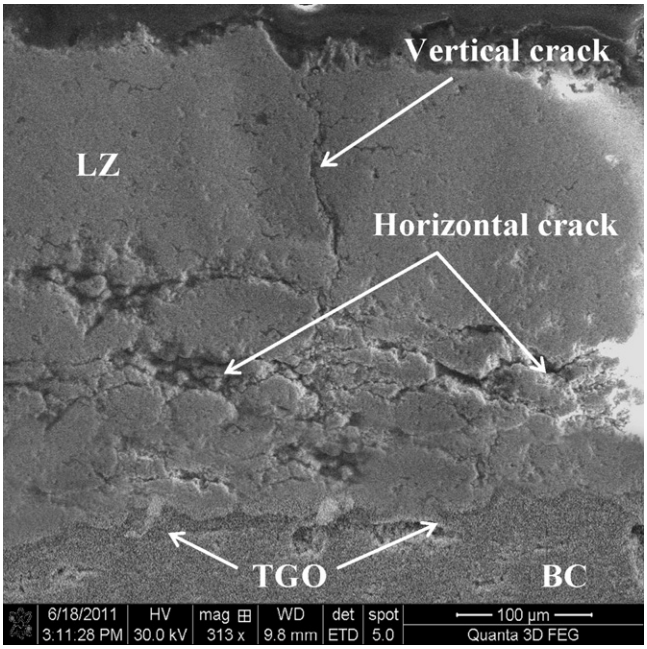

Fig. 27. Cross-sectional image LZ duplex coating after thermal cycling.

of expansion leads to the mismatch in coefficient of thermal expansion between the top ceramic layer and the BC. This thermal expansion mismatch results in an increase of residual stresses that can cause the failure of coatings.

4.3. The thermal cycling life of double ceramic layered coatings

The double ceramic layered coating survived more number of thermal cycles, compared to the LZ coating, which could be viewed in the graphical illustration shown in Fig. 17. The top surface of the thermally cycled double ceramic layered (Fig. 30) coating has a lot of cracks and the widths of the cracks are also large. The possible reason for the formation of microcracks is that the top ceramic layer is subjected to a tensile stress during heating [24]. The micrograph taken at the cross-section of the coating is shown in Fig. 31. The double ceramic layered coating shows cracks that have propagated from the surface and ended up in the interface between LZ and YSZ coatings. One can see extensive cracking right at the interface of the ceramic coatings (Fig. 31). This extensive cracking might have taken place due to thermal expansion mismatch, the high thickness of the coatings and the stress that occur due to TGO formation.

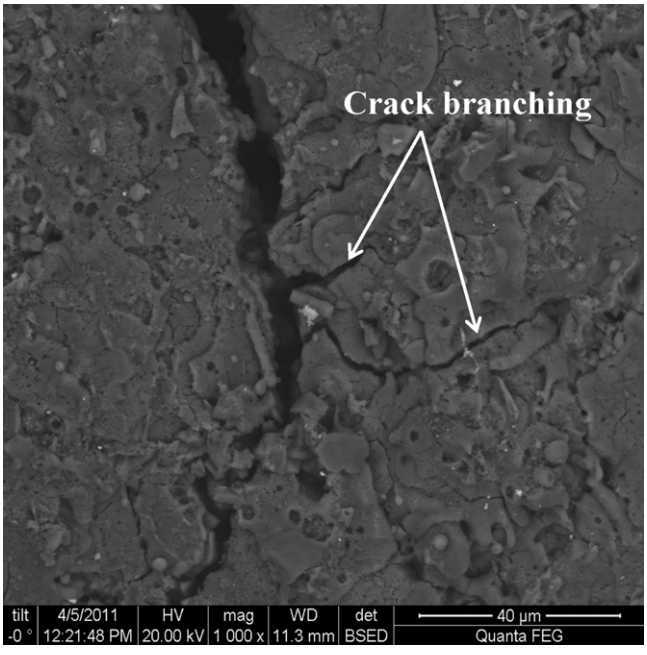

Fig. 26. High magnification image of top surface of LZ duplex coating after thermal cycling.

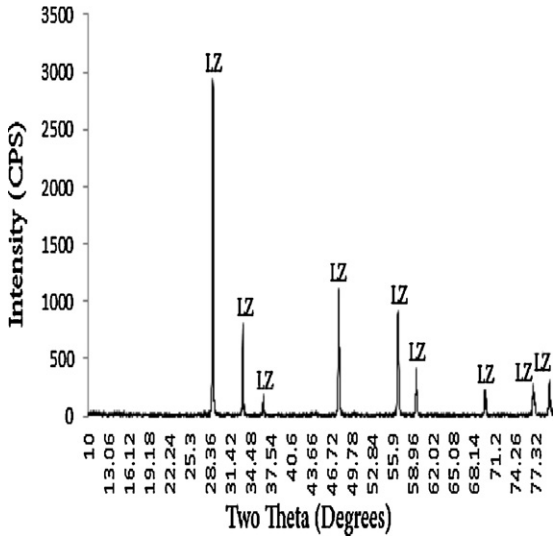

Fig. 28. XRD pattern LZ coating of after thermal cycling.

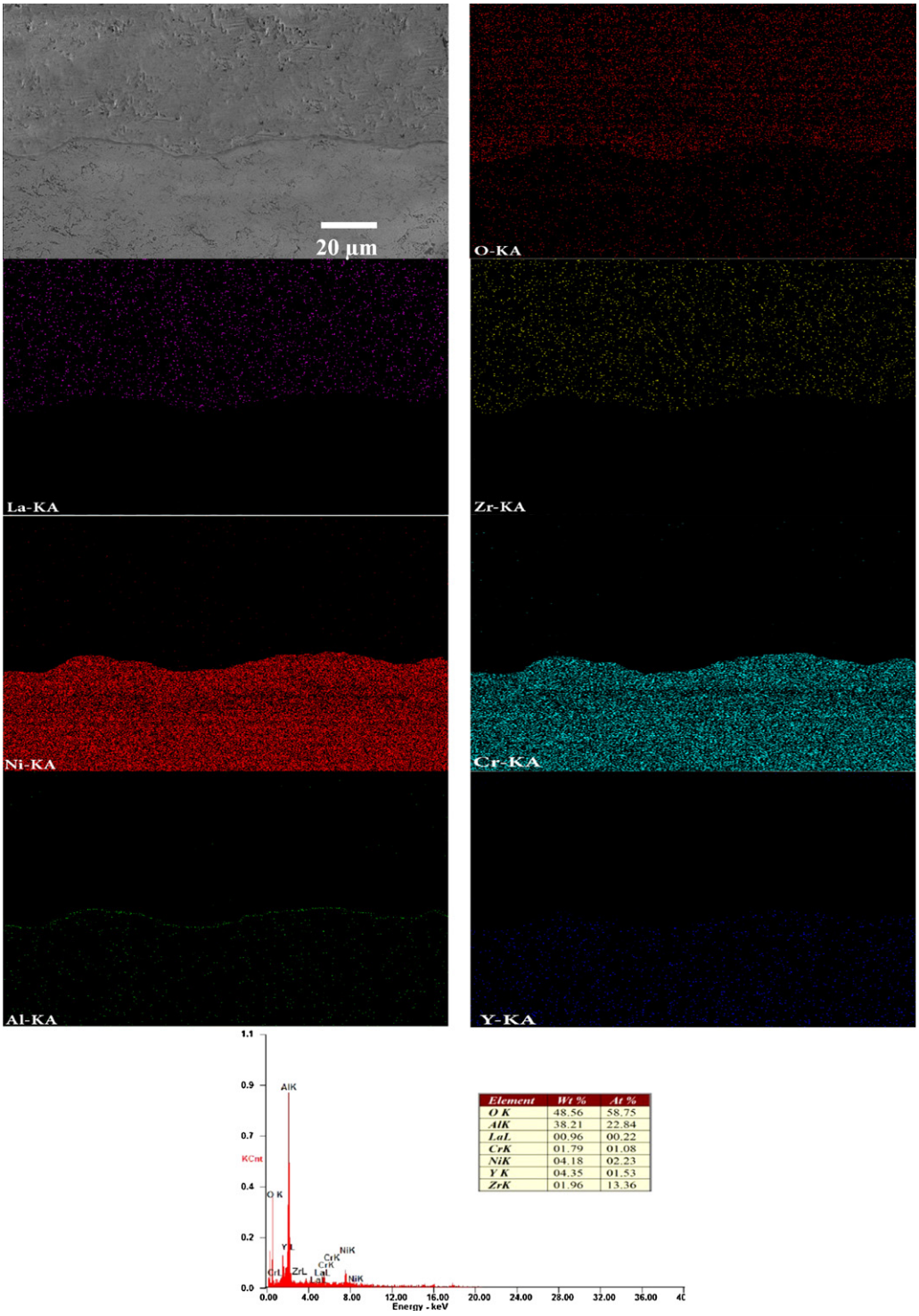

Fig. 29. EDS mapping results of LZ duplex coating after thermal cycling test.

4.3.1. TGO formation during the thermal cycling of double ceramic layered coating

The TGO formation can be seen at the YSZ–BC interface (subfigure in Fig. 31), with the thickness being 4–5 μm. One can see a number of vertical and transverse micro-cracks which are observed inside of the YSZ coating and they have further propagated down to the TGO layer. In this case, it is observed that the air goes through those large cracks propagating to the BC surface, and causes the oxidation of the BC. Therefore, a transverse crack to some extent, may lead to the spallation of the coating.

4.3.2. Factors influencing the thermal cycling life of double ceramic layered coating

The thickness of LZ coating is also one of the life controlling factors in the thermal cycling life of the double ceramic layered

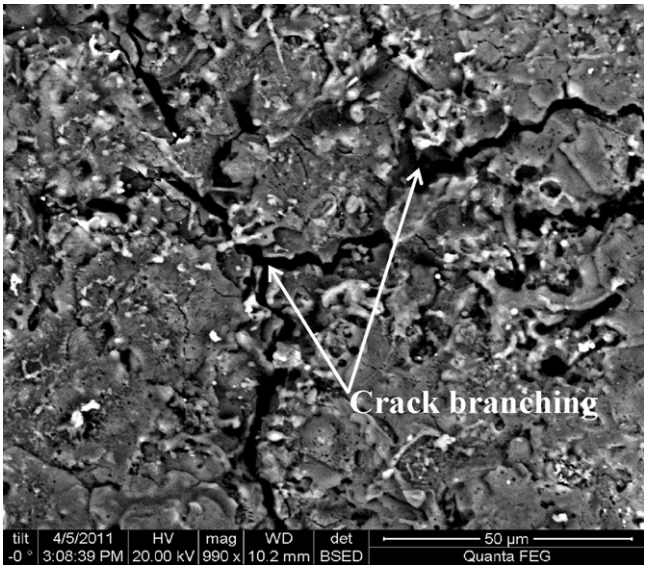

Fig. 30. Top surface of double ceramic layered coating after thermal cycling.

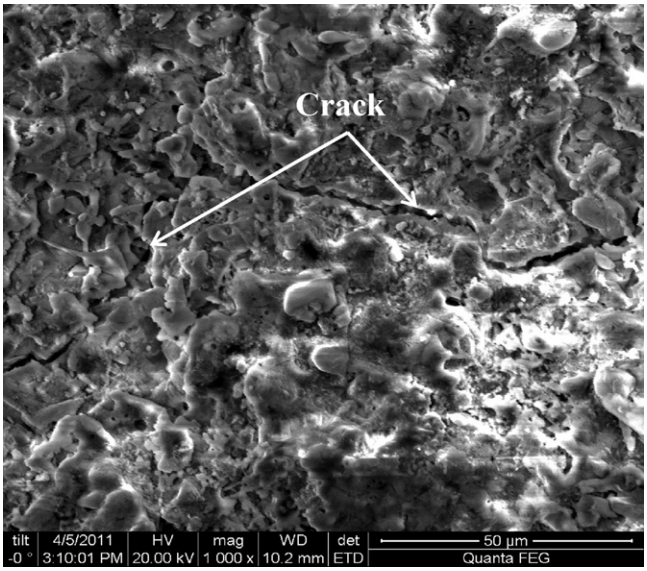

Fig. 32. Top surface of triple ceramic layered coating after thermal cycling.

coating [25]. The thickness of LZ coat in the case of the double ceramic layer system is 175 μm. This 175 μm thick LZ coat over the YSZ coat might have caused greater thermal gradients during the transient phase across coating thickness and consequently higher thermal stresses to occur within the coating and at the LZ–YSZ interface during thermal cycling. These two factors have caused double layered coating failure by spalling, tensile cracking at the LZ–YSZ interface and chipping on surface of the LZ coating. The interfacial thermal stress is also one of the factors for crack initiation and extension [26]. Fig. 31 exhibits a typical cleavage at the interface between the LZ and YSZ coatings, which is initiated by the compressive stresses developed during the cooling process. It is considered that when the compressive stresses are built up so much that they become larger than the bond strength of the LZ–YSZ coatings' interface during thermal cycling and the spallation occurs by the disconnection of the LZ coating from the YSZ coating.

4.4. Thermal cycling life of the triple ceramic layered coatings

Since the double ceramic layered coating failed at the interface between the LZ–YSZ coats, a 50 μm thick intermixed layer (LZ, 50 wt.% + YSZ, 50 wt.%) was sprayed in between the LZ and the YSZ coats. In this case the thickness of the LZ and YSZ coats was 150 μm. The top and cross-sectional features of the triple ceramic layered coating after thermal cycling are shown in Figs. 32 and 33, respectively. The induction of the intermixed ceramic has mitigated the crack

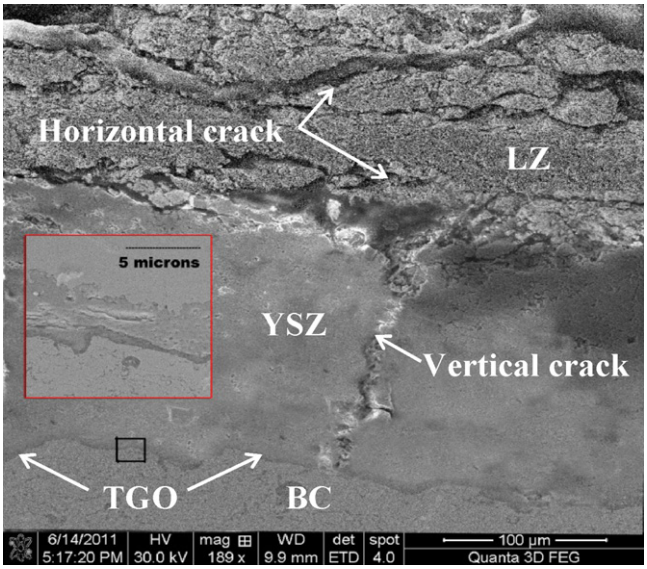

Fig. 31. Cross-sectional image of double ceramic layered coating after thermal cycling.

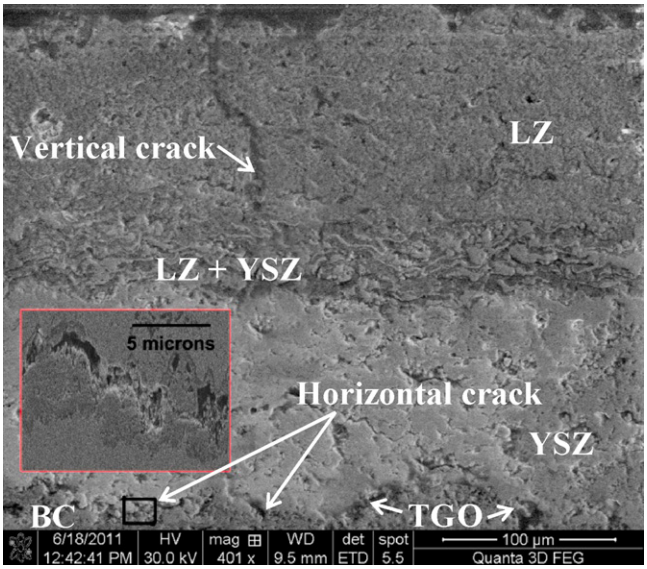

Fig. 33. Cross-sectional image of triple ceramic layered coating after thermal cycling.

propagation propensity. The thermal cycling and the oxidation resistance of the triple ceramic layered coating were found to be better than those of the YSZ duplex coatings (Figs. 17 and 18). Fig. 33 displays that there is no clear interface between the two adjacent layers. The gradient distribution of the two phases in the coating significantly eliminated the sharp interface of the double ceramic layered coating. The tensile stress at the ceramic coat-BC interface would be responsible in opening a crack parallel to the interface, resulting in crack propagation and a complete delamination [27].

4.4.1. Formation of cracks at the YSZ–BC interface during thermal cycling of triple ceramic layered coating

Note that the triple ceramic layered sample with a 50 μm thick inter mixed layer acted as a crack arresting barrier layer due to a decrease in the interfacial thermal stress and the thermal cycled specimen showed no delamination at the LZ–YSZ interface. Though the intermixed layer mentioned above mitigated the formation cracks at the LZ–YSZ interface, there were a lot of cracks observed at the YSZ–BC interface due to TGO formation. The TGO thickness was thin, around 4 μm and the transverse cracks were found to occur in the sample within the YSZ layer approximately 2 μm above the TGO layer and the transverse crack is more visible as could be observed from the subfigure in Fig. 33. The oxidation of BC could have resulted in a large in-plane compressive stress, inducing a significant out-of-plane tensile stress and producing delamination cracks parallel to the interface. These could open and propagate under repeated thermal cycling and cause a complete spallation [28]. Thus, the triple layer ceramic failed at the YSZ–BC interface.

4.5. Thermal cycling life of the four layered coatings

The top and cross-sectional views of the four layered coating are shown in Figs. 34 and 35. In this coating architecture an intermixed layer (YSZ, 50 wt.% + NiCrAlY, 50 wt.%) was sprayed (50 μm thickness) at the interface in between the YSZ coat and the BC. In this coating architecture also one can observe that there is no macro-interface (Fig. 35) between the YSZ and BC due to the annexation of an intermixed layer. It can be observed that BC changes its distribution pattern from a lamellar pattern to a dispersed pattern from the BC layer to the YSZ layer, and the YSZ layer also changes in the same way. Previous studies have shown that thermally activated time dependent (viscoplastic) deformations in the form of sintering, consolidation and stress–relaxation creep lead to the development of tensile stresses in the coating at the end of a heating–cooling cycle [29]. These tensile stresses are responsible for the initiation and growth of micro-cracks at the surface and at the TBC–BC interface eventually leading to delamination and structural failure of these TBCs.

4.5.1. Formation of cracks at the LZ–YSZ interface during thermal cycling of four layered coating

From Fig. 35 it is clear that the introduction of an intermixed layer at the YSZ–BC interface has potential to alleviate the interfacial failure during thermal cycling, but the failure of the coating took place right at the LZ–YSZ interface. The thermal cycling life and the oxidation resistance of the four layered coating are better than those of YSZ coating. It is believed that the intermixed layer (YSZ + NiCrAlY) had the compositive mechanical properties in strength and toughness, due to the microstructure improvement and relaxation of residual stress concentration [30]. The soft NiCrAlY phase in the intermixed layer dissipates the strain energy, thereby changing the cracking direction and passivating and ending the cracks. The cracks can be developed and propagated anywhere in this region independently, so that they are discontinuous. These discontinuous cracks in the interlayer release the thermal stress and prevent spallation at the coating interface [31]. The aforementioned composite strengthening and toughening effect led to the

Fig. 34. Top surface of four layered coating after thermal cycling.

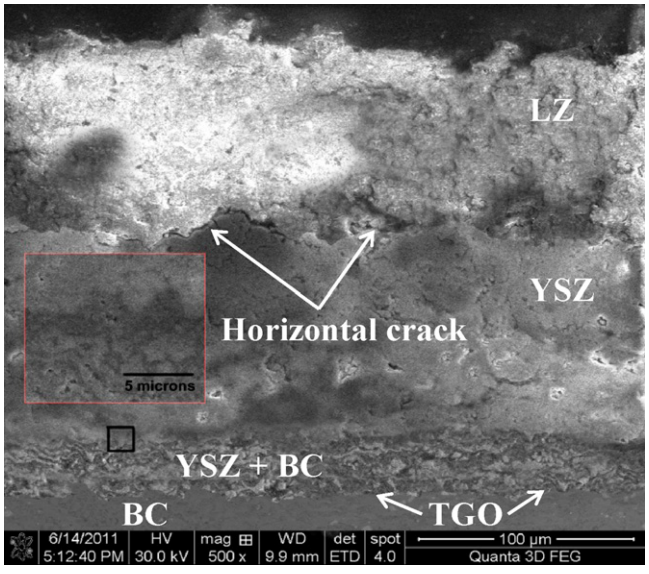

Fig. 35. Cross-sectional image of four layered coating after thermal cycling.

failure in another weak location of the coating, which obviously is the interface between the LZ–YSZ layers. From Fig. 35 one can see the propagation of a long longitudinal crack and sub cracks at the interface, which led to the spallation of the four layered coating at the LZ–YSZ interface.

4.6. Thermal cycling life of the five layered coating

From the study carried out on the thermal cycling behaviour of the three ceramic layered and four layered coating, it was inferred that the strengthening (providence of an intermixed layer) of one of the interfaces led to the weakening of the unmixed interface. Hence, the architecture of the five layered coating with two intermixed interface layers becomes inevitable to nurture the oxidation and thermal cycling resistances of LZ based coatings. The introduction of such interlayers led to a dramatic increase in the thermal cycling life of the lanthanum zircoante based coating as seen in Figs. 17 and 18. The five layered coating with stood 358 thermal cycles with a maximum oxidative weight gain of 1.2 mg/cm^2.

4.6.1. Influence of bond strength on the thermal cycling behaviour of the five layered coating

The tensile bond strength comparison chart for the LZ, YSZ and five layered coatings is shown in Fig. 15. According to previous studies, the residual stress levels present in the coatings can affect their thermal cycling life [32]. During the tensile bond strength test, the internal residual tensile stresses in the coating might get superimposed with the tensile loading, resulting in rapid separation or bond failure of the coatings. For the duplex coatings, because of the large difference of the thermal expansion coefficient of the top coat (LZ/YSZ) and the NiCrA1Y BC, the residual stress must be quite high. The high residual stresses and the sharp interface between the ceramic layer and the bond layer cause the earlier bond failure between the ceramic layer and the metallic layer. The thermal stresses can be decreased significantly by using intermixed interfacial layers and therefore, the bond strength can be improved significantly. The increase of bond strength is also because of the gradual change of the microstructure without sharp interface between different layers.

4.6.2. Influence of microhardness distribution on the thermal cycling behaviour of the five layered coating

The microhardness distributions of the duplex coatings and the five layered coating are displayed in Fig. 16. It can be observed from the figure that the microhardness changes gradually through the five layered coating, while a significant difference exists for the duplex coatings. The gradual variation of the microhardness for five layered coatings can reduce the large difference of the elastic modulus between ceramic and metal layers. The high bond strength and the gradual variation of the microhardness between the top ceramic coating and the substrate are beneficial to maintain the coating integrity under the strain generated by the alternating compressive and tensile stresses generated during the thermal cycling test.

4.6.3. Reasons behind the longer thermal cycling behaviour of the five layered coating

The top and cross-sectional morphologies of the thermal cycled five layered coating are shown in Figs. 36 and 37, respectively. The thermal cycled five layered coating did not undergo sintering as seen in Fig. 36. Fig. 37 suggests that the coating had spalled and the spallation took place at the top LZ layer. The TGO formation is there, but the thickness of the TGO is below 2 μm. The high oxidation resistance of the five layered coating is due to the sustenance of the non-oxygen transparent LZ coating for a longer period of time facilitated by the incorporation of the interfacial layers. Further, the cross-sectional micrograph of an uncoated IN738 alloy cycled up to 358 cycles is shown in Fig. 38, which indicates that without TBC, the IN738 alloy undergoes severe oxidation. The spallation of the five layered coating took place at the top LZ layer as seen in Fig. 37. Generally, the ceramic top layer of a coating is subjected to an in-plane compressive stress during heating. The axial stress pertinent to delamination is rather small. Thus, bi-axial compressive stress in the surface is the most important in regard to contribution of failure. From the context, the mechanism of the vertical crack formation has been elucidated as the following sequence [33]: during heating, the top surface of the five layered coating is in a large bi-axial compressive stress state. The stress causes non-linear deformation on the top surface of the coating. During cooling, the resulting strain causes the radial stress to become tensile. The change from compression to tension whose magnitude is large enough to exceed the fracture strength of the top ceramic layer (LZ layer) causes the vertical crack. The large tensile stress is limited to a shallow surface layer, which follows from the fact that the temperature decreases abruptly with increasing distance from the top surface and non-linear deformation is

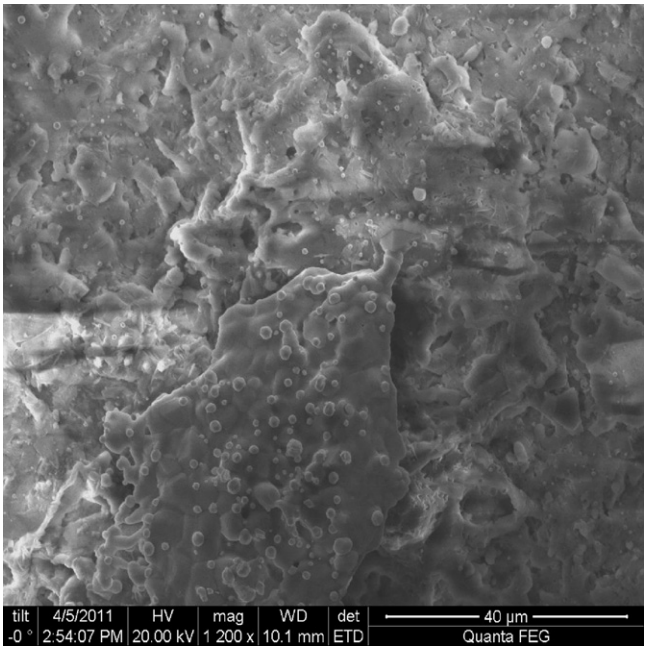

Fig. 36. Top surface of five layered coating after thermal cycling.

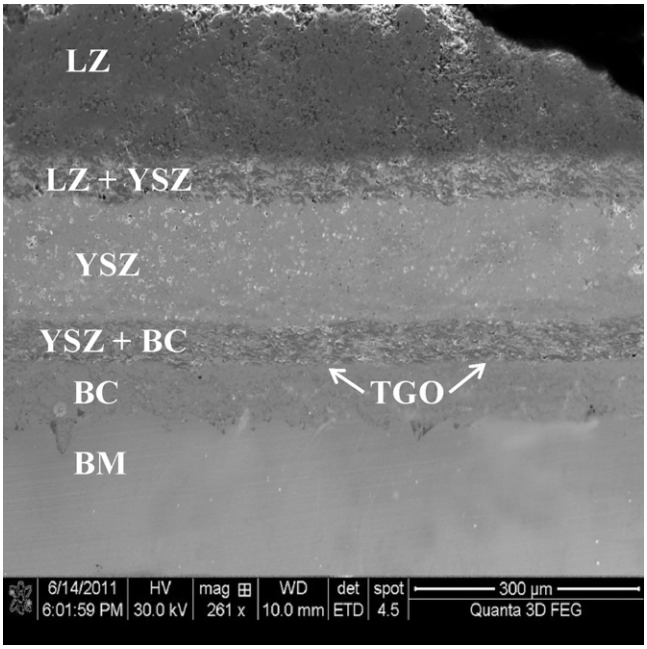

Fig. 37. Cross-sectional image of five ceramic layered coating after thermal cycling.

limited only to the shallow surface layer. Small cracks in the direction parallel to the surface are generated in the top layer. The number of the transverse cracks increases with the increase of thermal cycles and some link-up may lead to the localised fracture or chipping of the top coat. Therefore, the transverse cracks are to be generated during the heating phase. The orthogonal crack formation is considered to be due to a large tensile stress generated upon cooling because of inelastic compressive strain formed during heating in the top surface of the ceramic coating.

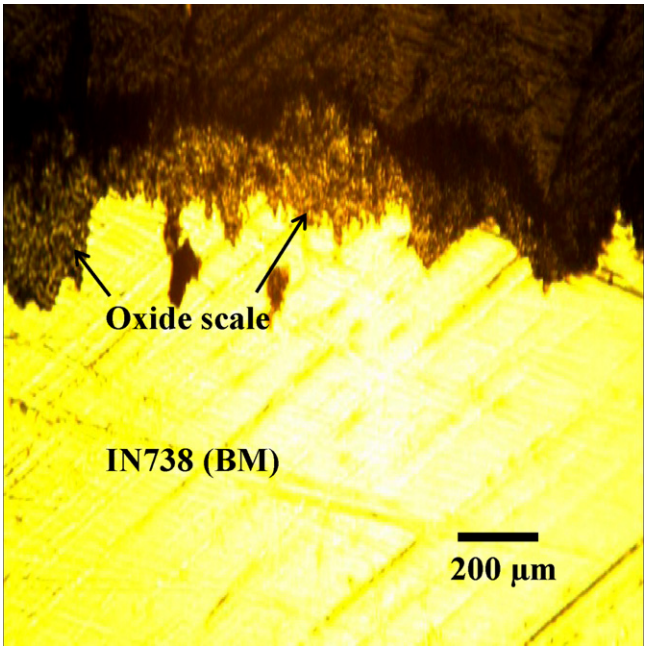

Fig. 38. Cross-sectional image of oxidised base metal after thermal cycling test.

5. Conclusions

- Thermal cycling tests were performed at 1280 °C to find the optimum coating architecture with lanthanum zirconate as the top coat material.
- The double ceramic layered coating with yttria stabilised zirconia (YSZ) as the intermediate layer between the LZ coat and bond coat (BC) survived 183 thermal cycles, which is 73 cycles higher and 68 cycles lower than those of LZ and YSZ coatings, respectively.
- The main failure mechanism of the double ceramic layered coating is the crack formation at the LZ–YSZ interface and severe bond coat oxidation.
- The induction of the 50 μm intermixed interlayer either at the LZ–YSZ interface or YSZ–BC interface increased the thermal cyclic life time of the coating longer than the life time of the YSZ coatings. But, the placement of intermixed layer at any one interface led to the weakening of the other interface.
- The thermal cycled five layered coating, which had two intermixed layers out lived the other considered coating architectures. The five layered coating withstood 358 thermal cycles with a maximum oxidative weight gain of 1.2 mg/cm^2.
- Within this five layered structure the intermixed interlayers provided sufficient toughness and strength during thermal cycling, while the LZ pyrochlore material applied on the top provides low thermal conductivity, low sintering ability, low oxygen transparency and high thermal stability.
- This five-layered coating architecture based on LZ pyrochlore/YSZ with intermixed interfacial layers revealed excellent high-temperature capability significantly better than the YSZ duplex coating and it is expected to improve the thermal capability of gas turbine engines during application.

Acknowledgements

The corresponding author wishes to express his sincere thanks to the Department of Science and Technology (DST), Government of India, New Delhi for the fellowship and financial support to carry out this investigation through sponsored fast track scheme for young scientists R&D Project No. SR/FT/ETA-01/2009. The authors record with gratitude the timely help rendered by Mr. Sundar and Mr. Murali of VB ceramic consultants, Chennai during the thermal cycling test.

References

[1] S. Sampath, Thermal sprayed ceramic coatings: fundamental issues and application considerations, Int. J. Mater. Prod. Technol. 35 (2009) 425–448.
[2] H. Dai, X. Zhong, J. Li, J. Meng, X. Cao, Neodymium–cerium oxide as new thermal barrier coating material, Surf. Coat. Technol. 201 (2006) 2527–2533.
[3] D.R. Clarke, S.R. Phillpo, Thermal barrier coating materials, Mater. Today 8 (2005) 22–29.
[4] J.Y. Li, H. Dai, Q. Li, X.H. Zhong, X.F. Ma, J. Meng, X.Q. Cao, Lanthanum zirconate nanofibers with high sintering-resistance, Mater. Sci. Eng. B 133 (2006) 209–212.
[5] R. Vassen, X. Cao, F. Tietz, D. Basu, D. Stover, Zirconates as new materials for thermal barrier coatings, J. Am. Ceram. Soc. 83 (2000) 2023–2028.

[6] H. Dai, X. Zhong, J. Li, Y. Zhang, J. Meng, X. Cao, Thermal stability of double-ceramic-layer thermal barrier coatings with various coating thickness, Mater. Sci. Eng. A 433 (2006) 1–7.
[7] Z. Xu, L. He, R. Mu, X. Zhong, Y. Zhang, J. Zhang, X. Cao, Double-ceramic-layer thermal barrier coatings of $La_2Zr_2O_7$/YSZ deposited by electron beam-physical vapor deposition, J. Alloys Compd. 473 (2009) 509–515.
[8] X.Q. Cao, R. Vassen, F. Tietz, D. Stoever, New double-ceramic-layer thermal barrier coatings based on zirconia-rare earth composite oxides, J. Eur. Ceram. Soc. 26 (2006) 247–251.
[9] C.S. Ramachandran, V. Balasubramanian, P.V. Ananthapadmanabhan, Synthesis, spheroidization and spray deposition of lanthanum zirconate using thermal plasma process, Surf. Coat. Technol. doi:10.1016/j.surfcoat.2011.10.052.
[10] J.Y. Li, H. Dai, X.H. Zhong, Y.F. Zhang, X.F. Ma, J. Meng, X.Q. Cao, Lanthanum zirconate ceramic toughened by $BaTiO_3$ secondary phase, J. Alloys Compd. 20 (2008) 406–409.
[11] C.S. Ramachandran, V. Balasubramanian, P.V. Ananthapadmanabhan, Multi-objective optimization of atmospheric plasma spray process parameters to deposit yttria-stabilized zirconia coatings using response surface methodology, J. Therm. Spray Technol. 20 (2010) 590–607.
[12] N.A. Fleck, A.C.F. Cocks, A multi-scale constitutive model for the sintering of an air-plasma-sprayed thermal barrier coating, and its response under hot isostatic pressing, J. Mech. Phys. Solids 57 (2009) 689–705.
[13] K. Takagi, D. Kudo, A. Kawasaki, Y. Harada, Microstructural dependency of thermal expansion and sintering shrinkage in plasma-sprayed zirconia coatings, Surf. Coat. Technol. 205 (2011) 4411–4417.
[14] C.H. Lee, H.K. Kim, H.S. Choi, H.S. Ahn, Phase transformation and bond coat oxidation behavior of plasma-sprayed zirconia thermal barrier coating, Surf. Coat. Technol. 124 (2000) 1–12.
[15] H.B. Guo, H. Murakami, S. Kuroda, Effect of hollow spherical powder size distribution on porosity and segmentation cracks in thermal barrier coatings, J. Am. Ceram. Soc. 89 (2006) 3797–3804.
[16] P.L. Ke, Y.N. Wu, Q.M. Wang, J. Gong, C. Sun, L.S. Wen, Study on thermal barrier coatings deposited by detonation gun spraying, Surf. Coat. Technol. 200 (2005) 2271–2276.
[17] D.B. Zhang, S.K. Gong, H.B. Xu, Effects of pre-oxide layer thickness on thermal cyclic behavior of thermal barrier coatings, Key Eng. Mater. 336 (2007) 1746–1749.
[18] A. Rabiei, A.G. Evans, Failure mechanisms associated with the thermally grown oxide in plasma-sprayed thermal barrier coatings, Acta Mater. 48 (2000) 3963–3976.
[19] W.R. Chen, X. Wu, B.R. Marple, P.C. Patnaik, The growth and influence of thermally grown oxide in a thermal barrier coating, Surf. Coat. Technol. 201 (2006) 1074–1079.
[20] A.G. Evans, D.R. Mumm, J.W. Hutchinson, G.H. Meier, F.S. Pettit, Mechanisms controlling the durability of thermal barrier coatings, Prog. Mater. Sci. 46 (2001) 505–553.
[21] F. Cao, B. Tryon, C.J. Torbet, T.M. Pollock, Microstructural evolution and failure characteristics of a NiCoCrAlY bond coat in hot spot cyclic oxidation, Acta Mater. 57 (2009) 3885–3894.
[22] H. Chen, Y. Gao, Y. Liu, H. Lu, Coprecipitation synthesis and thermal conductivity of $La_2Zr_2O_7$, J. Alloys Compd. 480 (2009) 843–848.
[23] T. Ohji, T. Sekino, K. Niihara, Thermal evolution of single phase lanthanum zirconate, Key Eng. Mater. 317 (2006) 31–36.
[24] H. Zhou, D. Yi, Z. Yu, L. Xiao, Preparation and thermophysical properties of CeO_2 doped $La_2Zr_2O_7$ ceramic for thermal barrier coatings, J. Alloys Compd. 438 (2007) 217–221.
[25] X. Bi, H. Xu, S. Gong, Investigation of the failure mechanism of thermal barrier coatings prepared by electron beam physical vapor deposition, Surf. Coat. Technol. 130 (2000) 122–127.
[26] C. Giolli, A. Scrivani, G. Rizzi, F. Borgioli, G. Bolelli, L. Lusvarghi, Failure mechanism for thermal fatigue of thermal barrier coating systems, J. Therm. Spray Technol. 18 (2009) 223–230.
[27] A. Sahin, F. Erdogan, On debonding of graded thermal barrier coatings, Int. J. Fract. 129 (2004) 341–359.
[28] S. Widjaja, A.M. Limarga, T.H. Yip, Oxidation behavior of a plasma-sprayed functionally graded ZrO_2/Al_2O_3 thermal barrier coating, Mater. Lett. 57 (2002) 628–634.
[29] W.R. Chen, X. Wu, B.R. Marple, P.C. Patnaik, Oxidation and crack nucleation/growth in an air-plasma-sprayed thermal barrier coating with NiCrAlY bond coat, Surf. Coat. Technol. 197 (2005) 109–115.
[30] S. Rangaraj, K. Kokini, Estimating the fracture resistance of functionally graded thermal barrier coatings from thermal shock tests, Surf. Coat. Technol. 173 (2003) 201–212.
[31] S. Rangaraj, K. Kokini, Fracture in single-layer zirconia (YSZ)-bond coat alloy (NiCoCrAlY) composite coatings under thermal shock, Acta Mater. 52 (2004) 455–465.
[32] M. Ranjbar-Far, J. Absi, G. Mariaux, F. Dubois, Simulation of the effect of material properties and interface roughness on the stress distribution in thermal barrier coatings using finite element method, Mater. Des. 31 (2010) 772–781.
[33] A. Kawasaki, R. Watanabe, Thermal fracture behavior of metal/ceramic functionally graded materials, Eng. Fract. Mech. 69 (2002) 1713–1728.